



Polyacrylamide-assisted freeze drying synthesis of hierarchical plate-arrayed LiV_3O_8 for high-rate lithium-ion batteries

S. Huang, Y. Lu, T.Q. Wang, C.D. Gu, X.L. Wang, J.P. Tu*

State Key Laboratory of Silicon Materials, Key Laboratory of Advanced Materials and Applications for Batteries of Zhejiang Province, Department of Materials Science and Engineering, Zhejiang University, Hangzhou 310027, China

HIGHLIGHTS

- We synthesize hierarchical LiV_3O_8 via polyacrylamide-assisted freeze drying method.
- The cyclic stability and rate capability are improved due to the special structure.
- This structure can facilitate the fast electron transport and Li ion diffusion.

ARTICLE INFO

Article history:

Received 26 October 2012

Received in revised form

7 February 2013

Accepted 12 February 2013

Available online 19 February 2013

Keywords:

Lithium trivanadium oxide

Plate-arrayed morphology

Lithium-ion battery

Cathode materials

ABSTRACT

Hierarchical plate-arrayed LiV_3O_8 is synthesized by freeze drying method with polyacrylamide (PAM) as surfactant followed by calcination at 500 °C. As a cathode material for lithium-ion batteries, the plate-arrayed LiV_3O_8 delivers an initial discharge capacity of 255.2 mAh g⁻¹ between 2.0 and 4.0 V at the current density of 50 mA g⁻¹, and possesses a capacity retention of 88.7% after 60 cycles. Moreover, high discharge capacities of 145.2, 133.7 and 111.8 mAh g⁻¹ can still be obtained after the 200th cycle at current densities of 600, 1500 and 3000 mA g⁻¹, respectively. Electrochemical impedance spectroscopy (EIS) test indicates that the LiV_3O_8 electrode always has very low impedance during the 3rd to 180th cycles. The improved electrochemical performance is attributed to the high crystallinity and uniform arrayed structure of LiV_3O_8 , which can facilitate the fast electron transport and Li ion diffusion in the electrode.

© 2013 Elsevier B.V. All rights reserved.

1. Introduction

With the popularization in portable electronic devices, electric vehicles (EVs) and hybrid electric vehicles (HEVs), lithium-ion batteries (LIBs) quickly occupy the market leading position due to their high energy density and long cycling life [1–3]. However, the positive electrode material is gradually becoming the bottleneck restriction of LIBs development because it is difficult to design a cathode which composes of environmentally benign, low-cost material that has its electrochemical potential μ_C well-matched to the HOMO of the electrolyte and allows access to two Li atoms per transition-metal cation [4]. During the past few years, olivine-type LiFePO_4 has been studied extensively [5–7]. It is expected to become commercially mature to replace the traditional LiMO_2 ($M = \text{Co}, \text{Ni}, \text{Mn}$) cathode materials [8–10].

Vanadium oxide can form layered compounds, and the element of vanadium has multiple valences [11]. For instance, the largest specific capacity can be obtained from the vanadium oxides where the vanadium is in its highest oxidation state, i.e. V^{5+} valence [12]. In particular, monoclinic lithium trivanadium oxide, LiV_3O_8 , has drawn more attentions recently and is regarded as a promising cathode material for LIBs because of its high specific capacity and electronic conductivity [13–16].

As is well known, the electrochemical performance of the cathode materials is influenced by the synthesis process, which has a great relationship with the microstructural and morphological characteristics [17,18]. Up to now, many strategies have been employed to synthesize the LiV_3O_8 compound, such as sol–gel process [19–21], hydrothermal process [22–24], solid-state reaction [13,14,25], rheological phase reaction [26,27], spray-drying synthesis [28], spray pyrolysis [29], freeze drying [30,31], combustion method [32] and RF magnetron sputtering [33]. However, the electrochemical performances, especially the capacity retention and high-rate capability of the LiV_3O_8 cathodes prepared by these methods are far from satisfactory. To exemplify,

* Corresponding author. Tel.: +86 571 87952856; fax: +86 571 87952573.
E-mail addresses: tujp@zju.edu.cn, tujplab@zju.edu.cn (J.P. Tu).

the LiV_3O_8 synthesized by a solid-state reaction has an initial specific discharge capacity of 273.6 mAh g^{-1} at a current density of 0.05 A g^{-1} , but it decreases to 234.5 mAh g^{-1} only after 30 cycles [25]. Recently, surface modification was adopted to improve the electrochemical performances at high current density [34]. Tian et al. employed a conducting polymer to incorporate polypyrrole (PPy) into the LiV_3O_8 active material, and the composite exhibited 189.0 mAh g^{-1} at the second cycle in the voltage range of 1.8–4.0 V at 0.5 C, and remained 169.6 mAh g^{-1} after 50 cycles [35]. The 1.0 wt. % AlPO_4 nanowire-coated LiV_3O_8 delivered an initial discharge capacity of 202.9 mAh g^{-1} at 1 C between 1.8 and 4.0 V. After 14 cycles, the discharge capacity increased to 232 mAh g^{-1} , and still remained 224 mAh g^{-1} after 60 cycles [36].

In this present work, we synthesized a hierarchical plate-arranged LiV_3O_8 using polyacrylamide (PAM) as surfactant by utilizing the freeze drying method. The structure, morphology and electrochemical performances, especially high-rate capability of the LiV_3O_8 were investigated.

2. Experimental

All chemicals were used directly without further purification. In a typical synthesis, 2.09 g of NH_4VO_3 was added into 100 mL of de-ionized water at 90°C under magnetic stirring until a bright yellow clear solution appeared, then 20 mL of 2.5 mg mL^{-1} homogeneous PAM (molecular weight ≥ 3 million) solution was added into it drop by drop and the mixed solution was vigorously stirred for 30 min. A stoichiometric amount of $\text{LiOH} \cdot \text{H}_2\text{O}$ was slowly added into the mixture, and then the mixed solution turned gradually to colorless transparent under stirring. Afterwards, the resultant solution was transferred to a refrigerator to freeze at -1°C for 24 h and the frozen precursor was further freeze dried at -50°C at 100 Pa for 24 h. Finally, the dried precursor was calcined at 400, 450, 500 and 550°C in air for 6 h to yield the final products. The as-synthesized oxides were named as LVO-P-400, LVO-P-450, LVO-P-500 and LVO-P-550 for short. The oxide powder was also prepared at 500°C using the same method without PAM, and the product was designated as LVO-N-500.

Thermogravimetric and differential thermal analysis (TG-DTA) of the hydroxide precursor were measured on a Pyris 1 TGA apparatus in the temperature range of 20 – 600°C at a heating rate of 7°C min^{-1} in air. The morphologies and structures of the as-synthesized powders were characterized using field emission scanning electron microscopy (FESEM, FEI SIRION), transmission electron microscopy (TEM, Tecnai G2 F20) and X-ray diffraction (XRD, Rigaku D/max-2550 with graphite monochromated CuK_α radiation). Rietveld refinement was performed on the XRD profiles to calculate the cell lattice parameters and the collected data were made using the software Maud.

Electrochemical performances of the LiV_3O_8 materials were investigated using CR2025 coin-type cell. The working electrodes were prepared by a slurry coating procedure. The slurry consisted of 80 wt. % oxide powder, 15 wt. % carbon conductive agent (acetylene black) and 5 wt. % polyvinylidene fluoride (PVDF) on aluminum foil. A metallic lithium foil served as the anode. 1 M LiPF_6 in ethylene carbonate (EC)-dimethyl carbonate (DMC) (1: 1 in volume) was used as the electrolyte, and a polypropylene micro-porous film (Cellgard 2300) as the separator. The cells were assembled in an argon-filled glove box with H_2O and O_2 concentrations below 1 ppm. The galvanostatic discharge-charge tests were performed on a LAND battery program-control test system between 2.0 and 4.0 V by applying the current densities from 50 to 3000 mA g^{-1} at room temperature. Cyclic

voltammetry (CV) test was carried out on an electrochemical workstation (CHI604B) in the potential window of 2.0–4.0 V (vs. Li/Li^+) at a scan rate of 0.1 mV s^{-1} . EIS measurements were performed on this apparatus using a three-electrode cell with the active material as the working electrode, metallic lithium foil as both the counter and reference electrodes. The amplitude of the AC signal was 5 mV over a frequency range from 100 kHz to 10 mHz at the stage of discharge.

3. Results and discussion

3.1. Material characterization

TG/DTA results of the dried precursor are illustrated in Fig. 1. The weight loss process can be simply divided into two stages. The first stage begins at 125°C and ends at 226°C with a weight loss of about 17%. Three obvious endothermic peaks appear at 166, 181 and 216°C in the DTA curve, which can be respectively attributed to the decomposition of PAM, the evaporation of adsorbed water and NH_3 , and the decomposition of NH_4VO_3 and LiOH . The second stage is from 226 to 359°C without any evident exo-/endothermic peaks, the weight loss can be ascribed to the following formation of LiV_3O_8 . Above 359°C , the smooth TG curve with constant weight indicates that no further phase transitions and reactions occur. So the calcination temperatures were chosen from 400 to 550°C .

Fig. 2 shows the XRD patterns of LiV_3O_8 powders synthesized at 400, 450, 500 and 550°C , and the refinement parameters are listed in Table 1. It can be seen that LVO-P-400 exhibits a pure layered-type LiV_3O_8 (Fig. 2a), which possesses a monoclinic crystalline structure and belongs to the $P2_1/m$ space group (JCPDS 72-1193). For LVO-P-450, LVO-P-500 and LVO-P-550, a $\text{Li}_{0.3}\text{V}_2\text{O}_5$ impurity phase (JCPDS 73-1670) is detected and the weight percentage of the phase within the composites is estimated using the Rietveld refinement. As shown in Fig. 2b and c, the content of $\text{Li}_{0.3}\text{V}_2\text{O}_5$ phase is 6.38 and 2.42 wt. % for LVO-P-450 and LVO-P-500, respectively. When the calcination temperature increases to 550°C , only 1.81 wt. % $\text{Li}_{0.3}\text{V}_2\text{O}_5$ can be found in the composite (Fig. 2d). As an intercalation material, the $\text{Li}_{0.3}\text{V}_2\text{O}_5$ phase has been reported by many groups [15,27,37,38–41]. Qiao et al. has synthesized the wafer-like porous $x\text{LiV}_3\text{O}_8-y\text{Li}_{0.3}\text{V}_2\text{O}_5$ composites by using a glycine-assisted solution route and found that the $\text{Li}_{0.3}\text{V}_2\text{O}_5$ phase could offer additional capacity to the total initial discharge

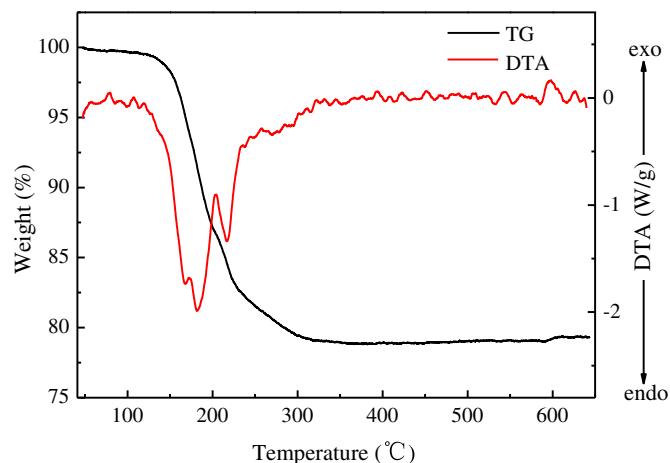


Fig. 1. TG and DTA data for the dried precursor with addition of PAM recorded from room temperature to 600°C at a heating rate of 7°C min^{-1} in air.

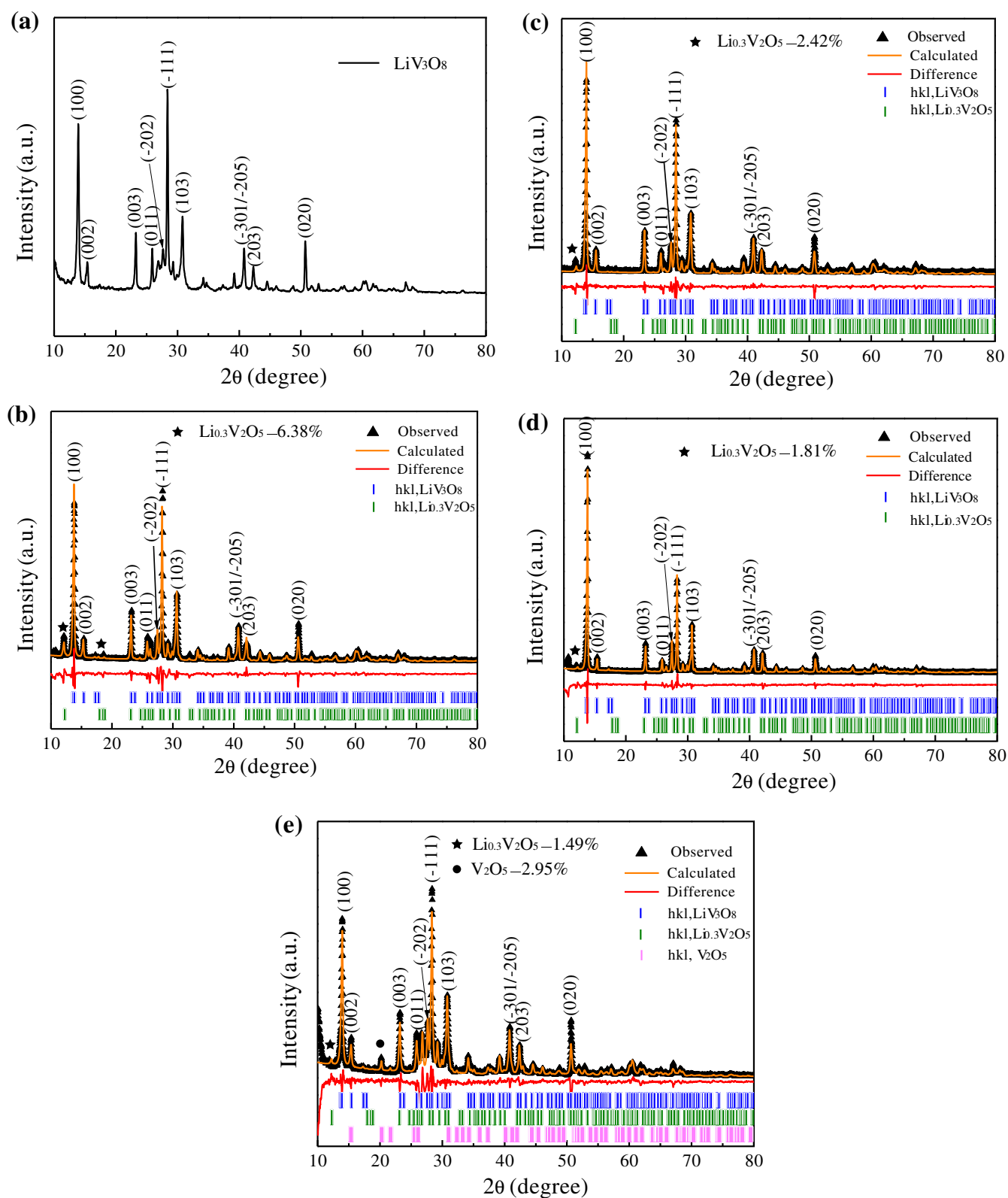


Fig. 2. (a) XRD pattern of LVO-P-400, and Rietveld-refined patterns of different LiV_3O_8 : (b) LVO-P-450, (c) LVO-P-500, (d) LVO-P-550 and (e) LVO-N-500.

Table 1
Refinement parameters for different LiV_3O_8 materials.

LiV_3O_8	<i>a</i>	<i>b</i>	<i>c</i>	β
450 °C	6.67025	3.59755	12.02859	107.88973
500 °C	6.68134	3.59946	12.03013	107.87051
550 °C	6.70024	3.60126	12.05414	107.95482
N-500 °C	6.63714	3.59942	12.05657	108.05063

capacity of the composites [37]. What's more, some groups have found an improved cycleability of LiV_3O_8 in the presence of $\text{Li}_{0.3}\text{V}_2\text{O}_5$ [28,42]. However, Wu et al. [43] and Zhou et al. [44] have shown that the presence of active phases such as $\text{Li}_{0.3}\text{V}_2\text{O}_5$ would degrade the cycling performance. Compared with other factors that mostly influence the cycleability of LiV_3O_8 materials, the effect of $\text{Li}_{0.3}\text{V}_2\text{O}_5$ impurity is little due to its small quantity. From Fig. 2e, another impurity peak corresponding to V_2O_5 phase is observed besides $\text{Li}_{0.3}\text{V}_2\text{O}_5$. V_2O_5 has been widely researched as a cathode material for LIBs [45–48]. Therefore, it can be expected that the presence of V_2O_5 phase will have a little influence on the electrochemical performances of LVO-N-500 due to the small content of 2.95 wt. %.

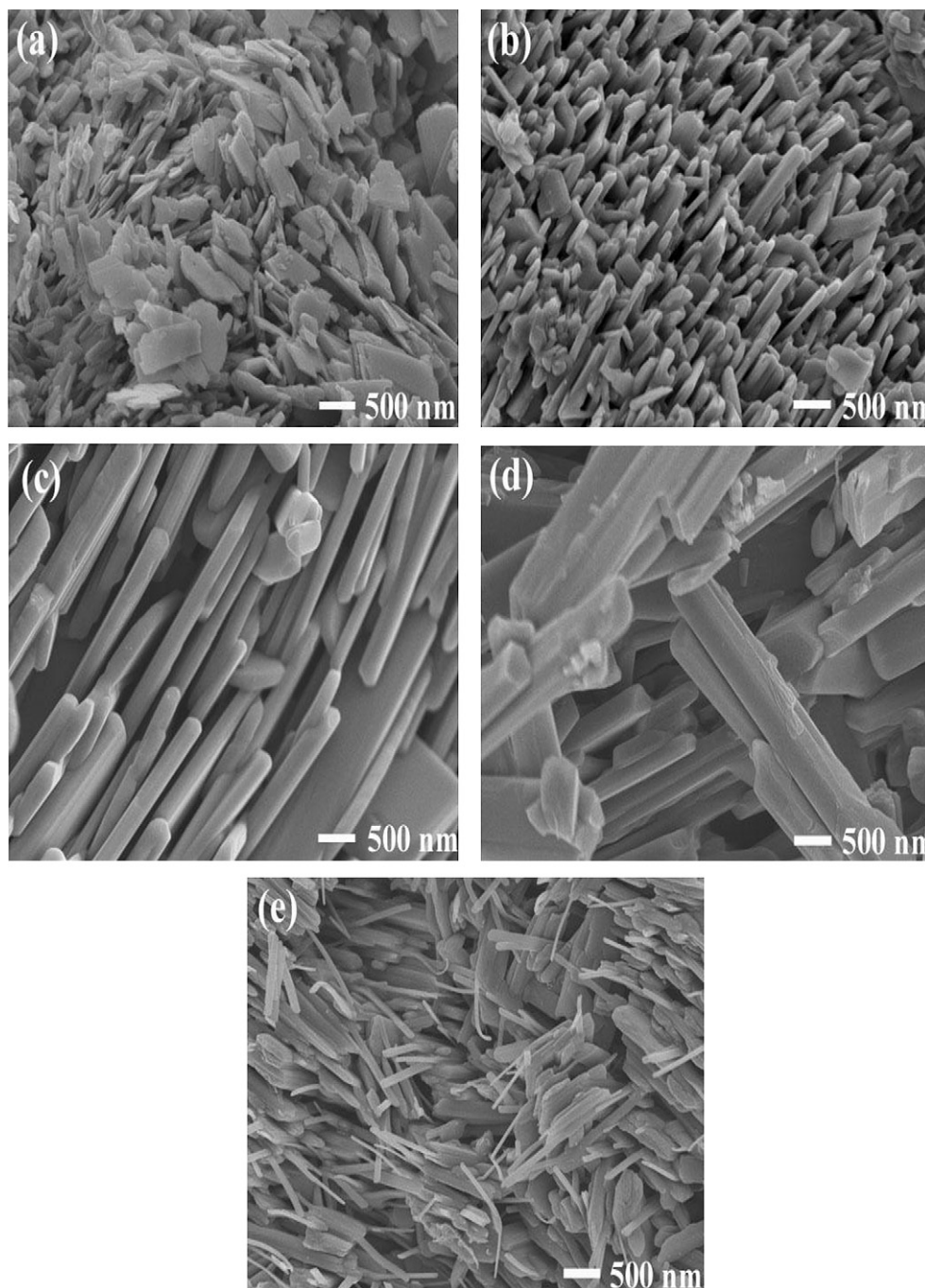


Fig. 3. SEM images of LiV_3O_8 powders: (a) LVO-P-400, (b) LVO-P-450, (c) LVO-P-500, (d) LVO-P-550 and (e) LVO-N-500.

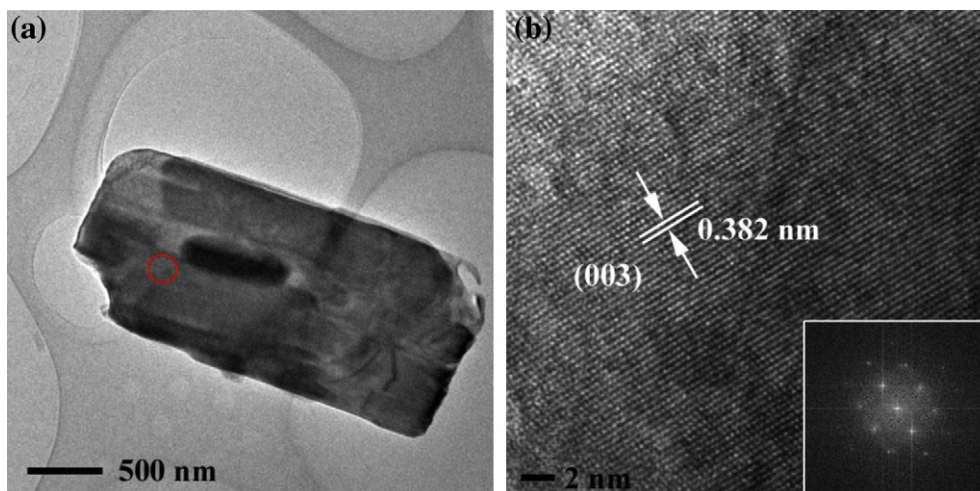


Fig. 4. (a) TEM and (b) HRTEM images of LVO-P-500. Inset in (b) shows the corresponding FFT pattern.

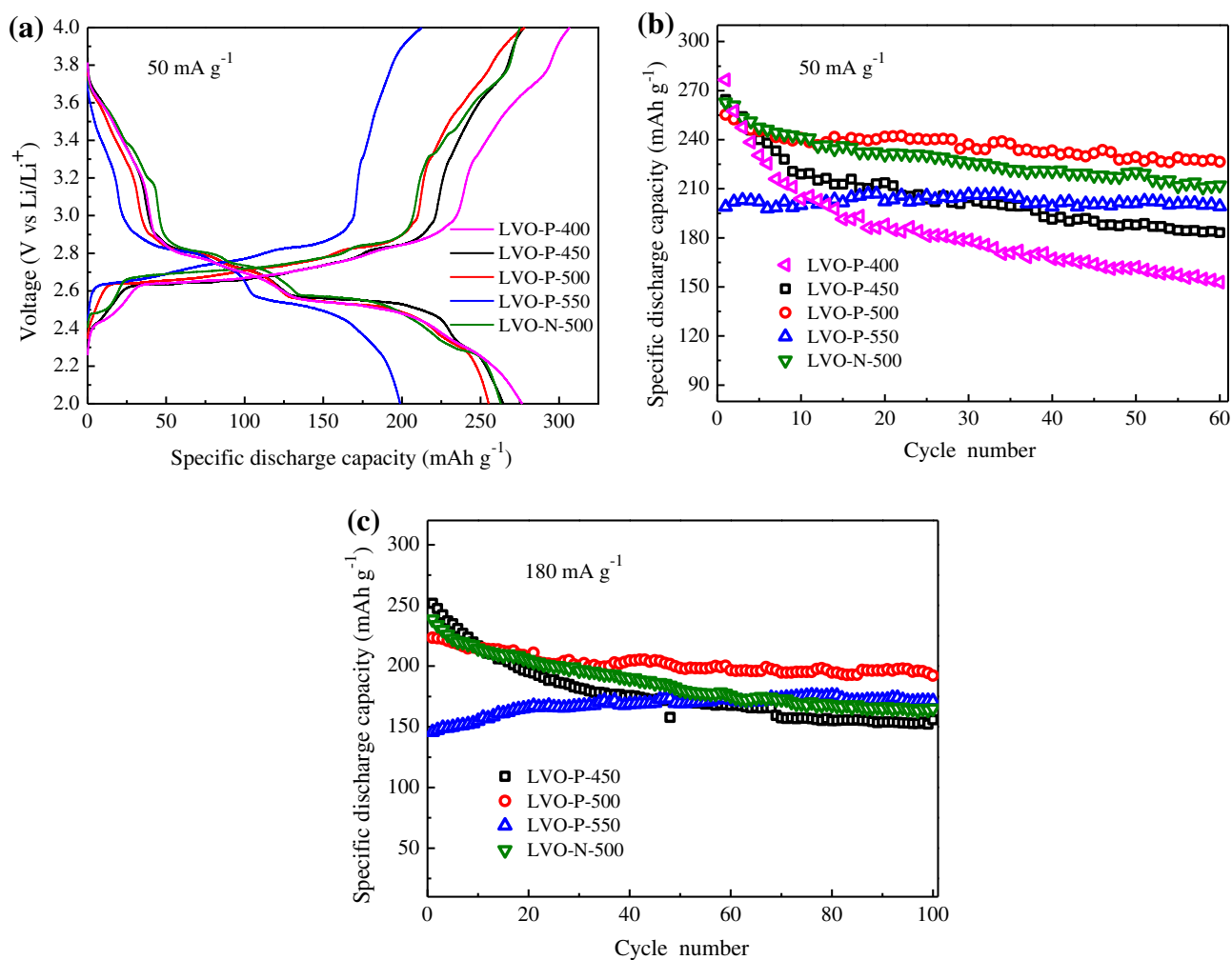


Fig. 5. (a) The first charge/discharge curves of LiV_3O_8 electrodes, (b) and (c) cycling performance at the current density of 50 mA g^{-1} and 180 mA g^{-1} respectively.

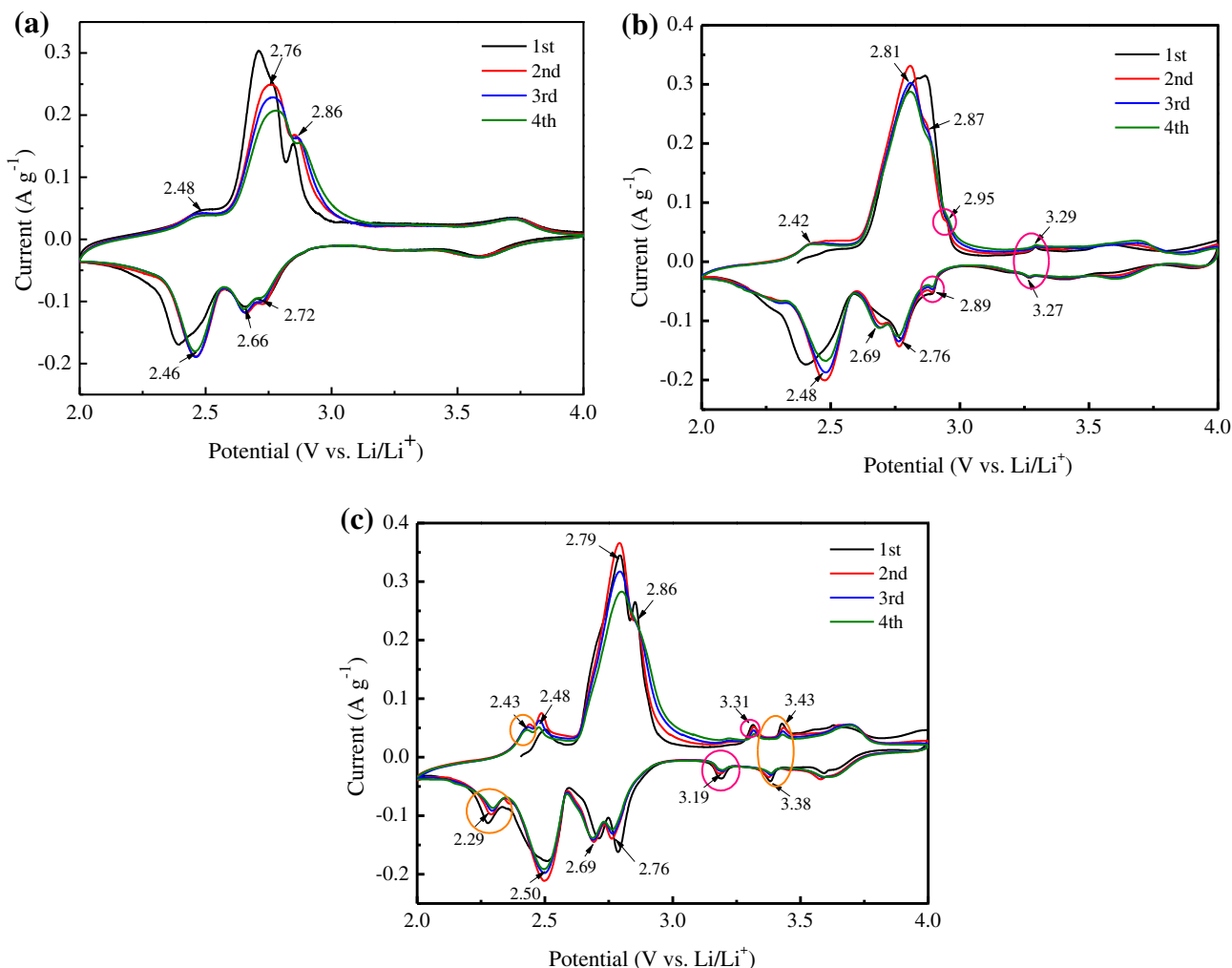


Fig. 6. CV curves of LiV_3O_8 electrodes at a scan rate of 0.1 mV s^{-1} in the potential range from 2.0 to 4.0 V (vs. Li/Li^+): (a) LVO-P-400, (b) LVO-P-500 and (c) LVO-N-500.

Fig. 3 shows the SEM images of the LiV_3O_8 particles synthesized under different conditions. It is obvious that LVO-P-400 is composed of accumulated thin plates, whose profiles are out-of-shape, indicating its low crystallinity (Fig. 3a). With increasing the temperature to 450°C , the arrayed plates are found to grow into compact and the plates are $180\text{--}270 \text{ nm}$ in thicknesses (Fig. 3b). What's more, the plates with inter-space between each other are connectedly arranged in the whole space, forming an array structure which is favorable for fast electron transportation and Li^+ diffusion. With further increasing the temperature to 500°C , the particles are basically remaining plate-arrayed configuration but growing into larger ones, with $200\text{--}300 \text{ nm}$ in thicknesses and a little longer length (Fig. 3c). It can be seen from Fig. 3d that the morphology of LVO-P-550 is completely rod-like with lengths of $2\text{--}8 \mu\text{m}$. This big rod is disadvantageous to electrochemical performances because it results in a long diffusion path for Li^+ insertion/extraction. Apparently, the calcination temperature has a great impact on the morphology of LiV_3O_8 particles, and this plate-arrayed structure can only be obtained between 450°C and 500°C with the surfactant of PAM. For LVO-N-500, as shown in Fig. 3e, it mainly shows a cluster of irregular and rambling rod morphology. In comparison with LVO-P-500 and LVO-N-500, it can be suspected that PAM has played two roles in the grain growth process: one is sticking the rods to

plates, and another is controlling the plates to form a regularly arrayed structure.

The hierarchical plate-arrayed LiV_3O_8 synthesized at 500°C is further analyzed by TEM, as displayed in Fig. 4. It shows a single plate with uneven surface whose length is about $2.5 \mu\text{m}$ and the width is $1.2 \mu\text{m}$. Such observation is in good match with the SEM images (Fig. 3). The high resolution TEM (HRTEM) image shows clear lattice fringes in the body part of the bulk indicated by a circular window in Fig. 4a. The 3.82 \AA spacing is in accordance with the interplanar distance of the (003) crystal plane of LiV_3O_8 (Fig. 4b). The result is further certified in the corresponding fast Fourier transform (FFT) pattern (inset in Fig. 4b), indicating the well-crystallized monoclinic LiV_3O_8 phase.

3.2. Electrochemical properties

Fig. 5 shows the electrochemical performances of LiV_3O_8 materials synthesized under different conditions. The initial charge/discharge curves of the electrodes between 2.0 and 4.0 V at 50 mA g^{-1} are shown in Fig. 5a. It can be seen that the voltage platform of LiV_3O_8 is mainly around $2.4\text{--}3.0 \text{ V}$, in which there are multiple phase transformation [49]. The LVO-P-400 electrode delivers an initial specific discharge capacity of 276.5 mAh g^{-1} ,

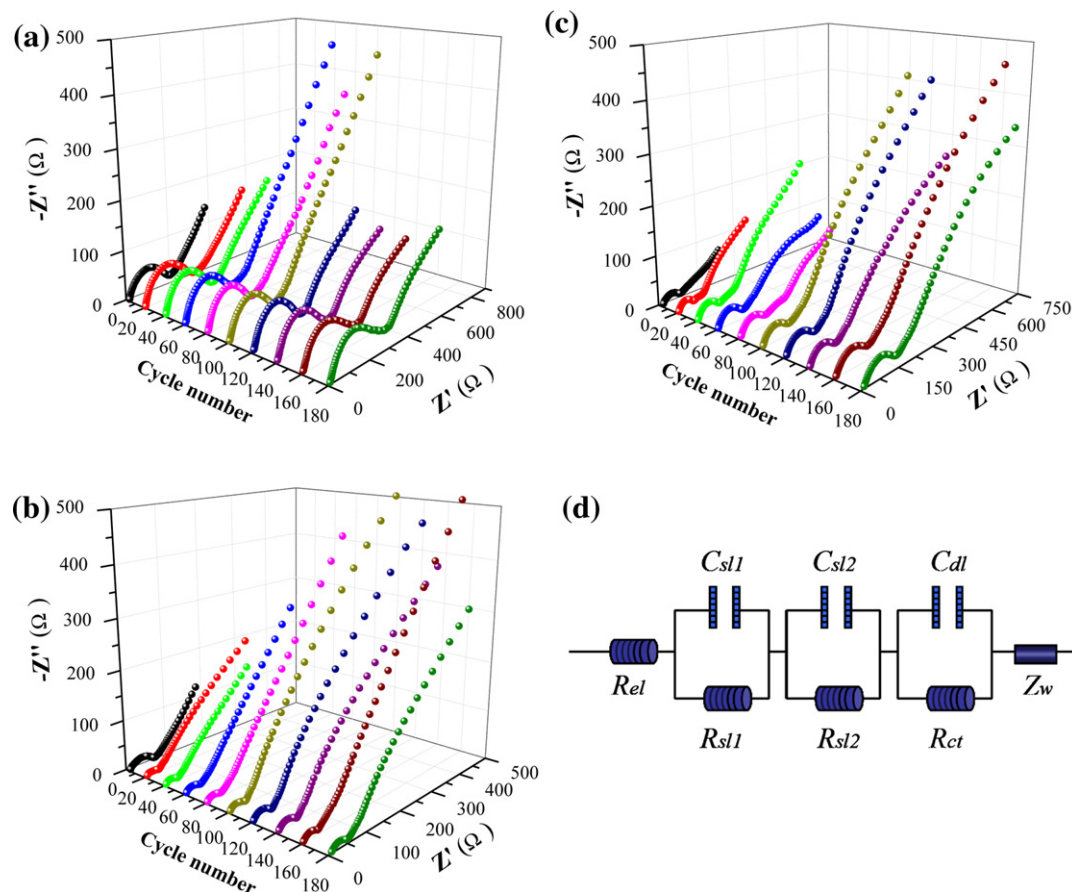


Fig. 7. Three-dimensional Nyquist plots for LiV_3O_8 electrodes after cycling at the discharge state of 2.50 V: (a) LVO-P-400, (b) LVO-P-500 and (c) LVO-N-500; (d) Equivalent circuit model for LiV_3O_8 electrodes.

high than LVO-P-450 (264.6 mAh g^{-1}), LVO-P-500 (255.2 mAh g^{-1}), LVO-P-550 (198.9 mAh g^{-1}) and LVO-N-500 (262.9 mAh g^{-1}), which is related to the small particle sizes. However, the discharge capacity of LVO-P-400 fades quickly during cycling, which is ascribed to its low degree of crystallinity (Fig. 5b). For LVO-P-500 with plate-arrayed structure, it can still retain a discharge capacity of 226.4 mAh g^{-1} after 60 cycles, whereas only 152.9 and 183.2 mAh g^{-1} can be sustained for LVO-P-400 and LVO-P-450, respectively. In addition, though the LVO-P-550 electrode has a good cycleability, the specific discharge capacity is much lower than others. As for LVO-N-500 without PAM, the cycling performance is inferior to the oxides with PAM. As shown in Fig. 5c, the LVO-P-450 electrode can still deliver an initial discharge capacity as high as 251.6 mAh g^{-1} when the current density is increased to 180 mA g^{-1} , but it quickly decreases to 155.7 mAh g^{-1} at the 100th cycle, which only preserves 61.9% of its initial capacity. While the LVO-P-500 electrode shows good cycling performance with high capacity retention of 86% after 100 cycles, better than LVO-N-500, whose capacity retention is only 69.3%. The improved electrochemical performances of the LVO-P-500 electrode can be mainly attributed to its high crystallinity and novel structure, which provides a fast transfer channel for electrons and shortens the diffusion path for Li^+ insertion/extraction in the connected arrayed structure with inter-space between these plates.

Fig. 6 shows the CV curves of LiV_3O_8 electrodes from 1st to 4th cycles in the potential range of 2.0–4.0 V (vs. Li/Li^+) at a scan rate

of 0.1 mV s^{-1} . From Fig. 6a, it can be seen that the LVO-P-400 electrode mainly shows three anodic peaks (2.48, 2.76 and 2.86 V) and three cathodic peaks (2.46, 2.66 and 2.72 V), which are well corresponding to the initial charge/discharge plateaus shown in Fig. 5a. The cathodic peaks at 2.66 and 2.72 V can be ascribed to the single-phase reaction with initial Li^+ insertion in the tetrahedral site, while the peak at 2.46 V corresponds to further Li^+ intercalation into tetrahedral sites with a two-phase transition from $\text{Li}_3\text{V}_3\text{O}_8$ to $\text{Li}_4\text{V}_3\text{O}_8$ [14,15,40,49,50]. For the LVO-P-500 electrode, as shown in Fig. 6b, besides the three main pairs of anodic/cathodic peaks, another two pairs of anodic/cathodic peaks (at 3.29, 3.27, 2.95 and 2.89 V) appear, which belong to the $\text{Li}_{0.3}\text{V}_2\text{O}_5$ active phase as observed in the XRD analysis. What's more, the good agreement of the CV curves demonstrates high structural reversibility and cyclic stability for the LVO-P-500 electrode. As for the LVO-N-500 electrode in Fig. 6c, the anodic peaks around 2.43 and 3.43 V and the cathodic peaks around 3.38 and 2.29 V marked by orange circles are attributed to another impurity V_2O_5 , which are similar to the previous reports [27,51]. The pair of anodic/cathodic peak at 3.31 and 3.19 V indicated by pink circles still belongs to $\text{Li}_{0.3}\text{V}_2\text{O}_5$ phase.

To identify the electrochemical reaction kinetics of electrode materials, EIS test was carried out to further study the LiV_3O_8 during the 3rd to 180th cycles. Fig. 7a–c shows the three-dimensional Nyquist plots for the LVO-P-400, LVO-P-500 and LVO-N-500 electrodes, respectively. It can be found that all of the

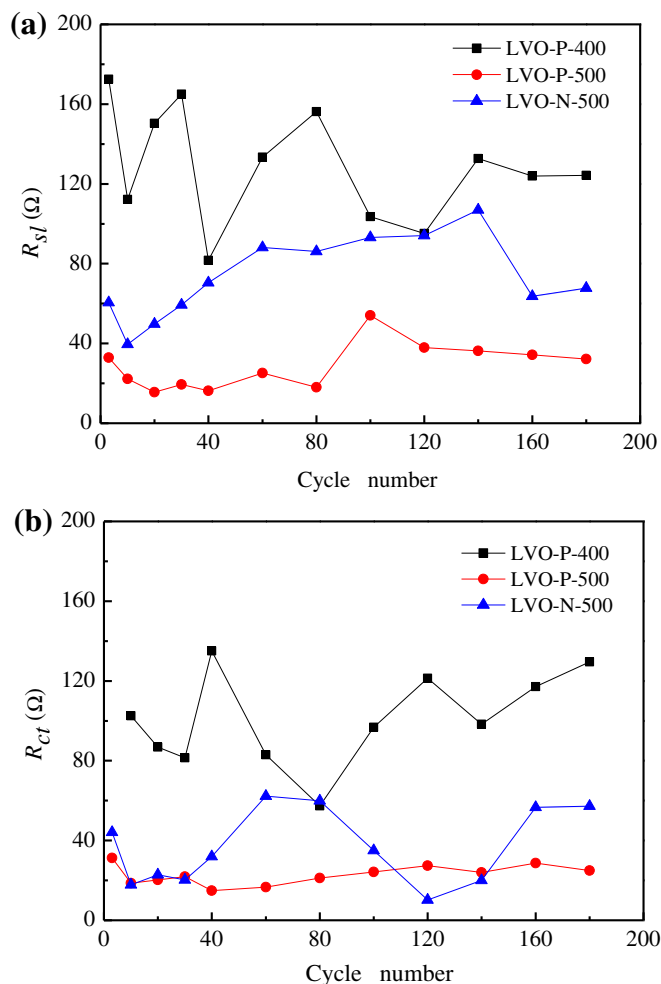


Fig. 8. Variation of (a) R_{sl} and (b) R_{ct} during cycling calculated from fitting the Nyquist plots.

plots consist of a small intercept at high frequency, two partially overlapped semicircles in the high- and medium-frequency regions and a long low-frequency line. Generally, the small intercept stands for the solution resistance of cell, and the first semicircle at high frequency is related to the resistance of surface-passivating layer. The second intermediate-frequency semicircle is indexed to the resistance of charge transfer on solid/electrolyte interface, and the following inclined line corresponds to the Warburg impedance of Li^+ diffusion in a solid material. To simulate the electrochemical impedance spectra, an equivalent circuit is adopted, as presented in Fig. 7d, where R_{el} indicates the solution resistance; $R_{sl}(i)$ and $C_{sl}(i)$ stand for the Li^+ migration resistance and the capacity of surface-passivating layer ($i = 1, 2$); while R_{ct} and C_{dl} designate the related charge transfer resistance and double-layer capacitance, respectively; and Z_W represents the diffusion-controlled Warburg impedance [52–54].

Fig. 8 reveals the fitting results of R_{sl} and R_{ct} electrical parameters in the equivalent circuit calculated by ZsimpWin computer program. As shown in Fig. 8a, the values of R_{sl} for the LVO-P-400 and LVO-N-500 electrodes show a trend of vibration during the whole discharge/charge cycles, which maybe result from the repetitive decomposition and formation of SEI film. While the variation of R_{sl} for the LVO-P-500 electrode is little,

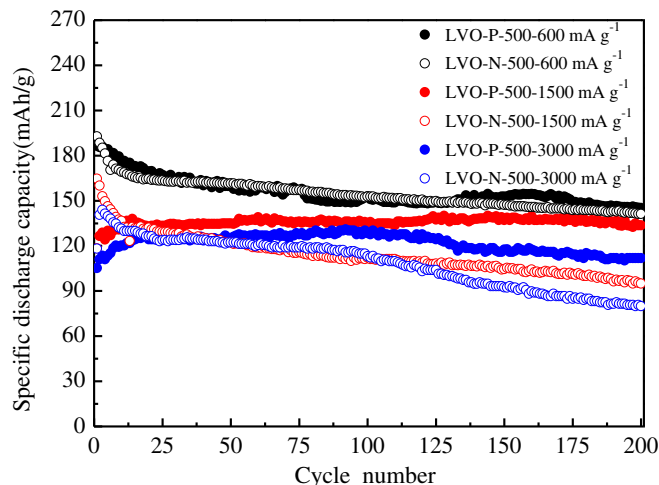


Fig. 9. Compared cycling performance between the LVO-P-500 and LVO-N-500 electrodes at various current densities between 2.0 and 4.0 V.

and the values are in the range of 16–54 Ω , indicating the formation of a stable surface film [37,53]. The trend of R_{ct} for the three electrodes is similar to that of R_{sl} (Fig. 8b). The LVO-P-400 electrode has a higher value than the other two ones, suggesting high polarization, which is related to its poor crystallinity. The 3rd value of R_{ct} for the LVO-P-500 and LVO-N-500 electrodes is 22.9 and 44.1 Ω , then after 180 cycles, the value of R_{ct} is 22.1 and 57.2 Ω , respectively. It is clearly that the LVO-P-500 electrode has the minimum R_{ct} value during cycling, indicating low polarization and in turn proving that the electron can transfer fast in this hierarchical plate-arrayed structure because the plates are connected between each other in the array.

In order to explore the rate performance, we compared the rate capability of the LVO-P-500 with that of LVO-N-500 electrode at various high current densities. As shown in Fig. 9, it can be seen that these two electrodes show very similar electrochemical behavior at a current density of 600 mA g^{-1} , but the capacity of LVO-N-500 drops sharply with cycling at high current densities, showing an inferior rate cycling performance compared to the LVO-P-500 electrode. Furthermore, even at current densities of 1500 mA g^{-1} and 3000 mA g^{-1} , high discharge capacity of 140 mAh g^{-1} at the 128th cycle and 130.2 mAh g^{-1} at the 81st cycle can still be obtained respectively for the LVO-P-500 electrode, whose overall capacity retention is 99 and 90% respectively from the 15th to 200th cycles. Table 2 shows the comparison of rate capability of our LVO-P-500 electrode with the previous reported LiV_3O_8 materials. The rate performance of the PAM-assisted LiV_3O_8 is superior to others. The improved rate capability can be attributed to the unique morphology. This plate-arrayed structure can contribute to fast electron transport, which can be demonstrated by the analysis results of R_{ct} in the EIS test. Moreover, the nanoscaled level in thickness for these plates contributes to shorten the diffusion path for Li^+ insertion/extraction, therefore enhancing the Li^+ diffusion kinetics [47,52]. Besides, the larger inter-space between the LiV_3O_8 plates in the array structure is favorable for increasing the interfacial area between the electrode and electrolyte and making full use of active material effectively. To some extent, it can also relieve the volume change during the Li^+ intercalation/extraction, thereby keeping the structural integrity during the discharge/charge processes.

Table 2Comparison of rate capabilities of LiV_3O_8 prepared by different methods.

Synthesis method	Composition	Temperature (°C)/time (h)	Particle morphology	Voltage window (V)	Current density	Capacity (mAh g^{-1})
Peroxide sol–gel method with oxidative polymerization of pyrrole monomer [35]	LiV_3O_8 –polypyrrole (PPy) composite	300/16	Amorphous PPy and LiV_3O_8 particles	1.8–4.0	2 C 5 C	162.8(2)–152.1 (50) 114.8(1)–100 (50)
Surfactant-assisted polymer precursor method [40]	LiV_3O_8	550/2	Rods; diameter < 1 μm	2.0–4.0	240 mA g^{-1}	152(2)–152 (60)
Solution method with PEG Ref. [55]	LiV_3O_8	500/2	Nanosheet-structure	1.5–4.0	1000 mA g^{-1}	162(2)–157 (100)
Hydrothermal method [56]	LiV_3O_8 /Carbon composite	450/10	Nanosheet	1.5–4.0	5 C 10 C 20 C	118(2)–110 (250) 104(2)–104 (250) 65(2)–82 (250)
Sol–gel method [57]	$(1-x)\text{LiV}_{2.94}\text{Zr}_{0.06}\text{O}_8$ $\cdot x\text{Li}_{0.3}\text{V}_2\text{O}_5$	550/12	Irregular bulk	1.8–4.0	1.0 C	169(1)–173.1 (150)
This work	$(1-x)\text{LiV}_3\text{O}_8$ $\cdot x\text{Li}_{0.3}\text{V}_2\text{O}_5$	500/6	Hierarchical plate-array	2.0–4.0	1500 mA g^{-1} 3000 mA g^{-1}	126.6(2)–133.7 (200) 111(2)–111.8 (200)

4. Conclusions

The hierarchical plate-arrayed LiV_3O_8 was successfully synthesized by PAM-assisted freeze drying method. The LiV_3O_8 fabricated at 500 °C shows uniform plate-arrayed structure with large inter-space between these plates, which can increase the interfacial area between the electrode and electrolyte and contribute to fast electron transport and Li^+ diffusion, thus leading to improved electrochemical performances. Even after 200 cycles, high discharge capacities of 145.2, 133.7 and 111.8 mAh g^{-1} can still be obtained at current densities of 600, 1500 and 3000 mA g^{-1} , respectively. The plate-arrayed LiV_3O_8 is a promising candidate as the cathode material for high-power LIBs.

Acknowledgments

This work was supported by the National Science and Technology Support Program (2012BAK30B04-05) and Key Science and Technology Innovation Team of Zhejiang Province (2010R50013). The authors also thank the help of Mr. Wei Huang of operating the TEM.

References

- [1] C. Liu, F. Li, L.-P. Ma, H.-M. Cheng, *Adv. Mater.* 22 (2010) E28.
- [2] J. Hassoun, P. Reale, B. Scrosati, *J. Mater. Chem.* 17 (2007) 3668.
- [3] A.Q. Pan, J.-G. Zhang, Z.M. Nie, G.Z. Cao, B.W. Arey, G.S. Li, S.-Q. Liang, J. Liu, *J. Mater. Chem.* 20 (2010) 9193.
- [4] J.B. Goodenough, Y. Kim, *Chem. Mater.* 22 (2010) 587.
- [5] F. Yu, J.-J. Zhang, Y.-F. Yang, G.-Z. Song, *J. Mater. Chem.* 19 (2009) 9121.
- [6] J.Y. Xiang, J.P. Tu, L. Zhang, X.L. Wang, Y. Zhou, Y.Q. Qiao, Y. Lu, *J. Power Sources* 195 (2010) 8331.
- [7] W.L. Liu, J.P. Tu, Y.Q. Qiao, J.P. Zhou, S.J. Shi, X.L. Wang, C.D. Gu, *J. Power Sources* 196 (2011) 7728.
- [8] Y. Takahashi, S. Tode, A. Kinoshita, H. Fujimoto, I. Nakane, S. Fujitani, *J. Electrochem. Soc.* 155 (2008) A537.
- [9] X.X. Shi, C.W. Wang, X.L. Ma, J.T. Sun, *Mater. Chem. Phys.* 113 (2009) 780.
- [10] B. Ammundsen, J. Desilvestro, T. Groutso, D. Hassell, J.B. Metson, E. Regan, R. Steiner, P.J. Pickering, *J. Electrochem. Soc.* 147 (2000) 4078.
- [11] J.W. Fergus, *J. Power Sources* 195 (2010) 939.
- [12] V. Manev, A. Momchilov, A. Nassalevska, G. Pistoia, M. Pasquali, *J. Power Sources* 54 (1995) 501.
- [13] G.Q. Liu, C.L. Zeng, K. Yang, *Electrochim. Acta* 47 (2002) 3239.
- [14] J. Kawakita, T. Miura, T. Kishi, *J. Power Sources* 83 (1999) 79.
- [15] A.Q. Pan, J. Liu, J.-G. Zhang, G.Z. Cao, W. Xu, Z.M. Nie, X. Jie, D.W. Choi, B.W. Arey, C.M. Wang, S.Q. Liang, *J. Mater. Chem.* 21 (2011) 1153.
- [16] X.-W. Gao, J.-Z. Wang, S.-L. Chou, H.-K. Liu, *J. Power Sources* 220 (2012) 47.
- [17] J.J. Feng, X.Z. Liu, X.M. Zhang, J.Z. Jiang, J. Zhao, M. Wang, *J. Electrochem. Soc.* 156 (2009) A768.
- [18] K. West, B. Zachau-Christiansen, S. Skaarup, Y. Saidi, J. Barker, I.I. Olsen, R. Pynenburg, R. Koksang, *J. Electrochem. Soc.* 143 (1996) 820.
- [19] H. Ma, Z.Q. Yuan, F.Y. Cheng, J. Liang, Z.L. Tao, J. Chen, *J. Alloys Compd.* 509 (2011) 6030.
- [20] A. Deptula, M. Dubarry, A. Noret, J. Gaubicher, T. Olczak, W. Łada, D. Guyomard, *Electrochem. Solid State Lett.* 9 (2006) A16.
- [21] L. Liu, L.F. Jiao, Y.H. Zhang, J.L. Sun, L. Yang, Y.L. Miao, H.T. Yuan, Y.M. Wang, *Mater. Chem. Phys.* 111 (2008) 565.
- [22] H.Y. Xu, H. Wang, Z.Q. Song, Y.W. Wang, H. Yan, M. Yoshimura, *Electrochim. Acta* 49 (2004) 349.
- [23] X.L. Li, P.P. Li, M. Luo, X.Y. Chen, J.J. Chen, *J. Solid State Electrochem.* 14 (2010) 1325.
- [24] J.Q. Xu, H.L. Zhang, T. Zhang, Q.Y. Pan, Y.H. Gui, *J. Alloys Compd.* 467 (2009) 327.
- [25] W.Z. Wu, J. Ding, H.R. Peng, G.C. Li, *Mater. Lett.* 65 (2011) 2155.
- [26] Q.Y. Liu, H.W. Liu, X.W. Zhou, C.J. Cong, K.L. Zhang, *Solid State Ionics* 176 (2005) 1549.
- [27] Y.Q. Qiao, X.L. Wang, J.P. Zhou, J. Zhang, C.D. Gu, J.P. Tu, *J. Power Sources* 198 (2012) 287.
- [28] N. Tran, K.G. Bramnik, H. Hibst, J. Pröll, N. Mronja, M. Holzapfel, W. Scheifele, P. Novák, *J. Electrochem. Soc.* 155 (2008) A384.
- [29] S.H. Ju, Y.C. Kang, *Electrochim. Acta* 55 (2010) 6088.
- [30] H.M. Liu, Y.G. Wang, W.S. Yang, H.S. Zhou, *Electrochim. Acta* 56 (2011) 1392.
- [31] O.A. Brylev, O.A. Shlyakhtin, A.V. Egorov, Y.D. Tretyakov, *J. Power Sources* 164 (2007) 868.
- [32] Y.-C. Si, L.-F. Jiao, H.-T. Yuan, H.-X. Li, Y.-M. Wang, *J. Alloys Compd.* 486 (2009) 400.
- [33] Q. Shi, R.Z. Hu, L.Z. Ouyang, M.Q. Zeng, M. Zhu, *Electrochem. Commun.* 11 (2009) 2169.
- [34] Z.H. Chen, Y. Qin, K. Amine, Y.-K. Sun, *J. Mater. Chem.* 20 (2010) 7606.
- [35] F.H. Tian, L. Liu, Z.H. Yang, X.Y. Wang, Q.Q. Chen, X.Y. Wang, *Mater. Chem. Phys.* 127 (2011) 151.
- [36] L.F. Jiao, L. Liu, J.L. Sun, L. Yang, Y.H. Zhang, H.T. Yuan, Y.M. Wang, X.D. Zhou, *J. Phys. Chem. C* 112 (2008) 18249.
- [37] Y.Q. Qiao, J.P. Tu, X.L. Wang, J. Zhang, Y.X. Yu, C.D. Gu, *J. Phys. Chem. C* 115 (2011) 25508.
- [38] T.J. Patey, S.H. Ng, R. Büchel, N. Tran, F. Krumeich, J. Wang, H.K. Liu, P. Novák, *Electrochem. Solid-State Lett.* 11 (2008) A46.
- [39] H.-L. Zhang, J.R. Neilson, D.E. Morse, *J. Phys. Chem. C* 114 (2010) 19550.
- [40] A. Sakunthala, M.V. Reddy, S. Selvasekarapandian, B.V.R. Chowdari, P.C. Selvin, *J. Phys. Chem. C* 114 (2010) 8099.
- [41] Y.M. Liu, X.C. Zhou, Y.L. Guo, *Electrochim. Acta* 54 (2009) 3184.
- [42] M. Dubarry, J. Gaubicher, P. Moreau, D. Guyomard, *J. Electrochem. Soc.* 153 (2006) A295.
- [43] F. Wu, L. Wang, C. Wu, Y. Bai, F. Wang, *Mater. Chem. Phys.* 115 (2009) 707.
- [44] Y. Zhou, H.-F. Yue, X.-Y. Zhang, X.-Y. Deng, *Solid State Ionics* 179 (2008) 1763.
- [45] H.B. Zhao, L.Y. Pan, S.Y. Xing, J. Luo, J.Q. Xu, *J. Power Sources* 222 (2013) 21.
- [46] K. Dewangan, N.N. Sinha, P.G. Chavan, P.K. Sharma, A.C. Pandey, M.A. More, D.S. Joag, N. Munichandraiah, N.S. Gajbhiye, *Nanoscale* 4 (2012) 645.
- [47] X.-F. Zhang, K.-X. Wang, X. Wei, J.-S. Chen, *Chem. Mater.* 23 (2011) 5290.
- [48] K.-I. Park, H.-M. Song, Y. Kim, S. Mho, W.I. Cho, I.-H. Yeo, *Electrochim. Acta* 55 (2010) 8023.
- [49] R. Benedek, M.M. Thackeray, L.H. Yang, *J. Power Sources* 81 (1999) 487.
- [50] S. Jouanneau, A. Le Gal La Salle, A. Verbaere, D. Guyomard, *J. Electrochem. Soc.* 152 (2005) A1660.
- [51] A. Sakunthala, M.V. Reddy, S. Selvasekarapandian, B.V.R. Chowdari, P.C. Selvin, *Energy Environ. Sci.* 4 (2011) 1712.
- [52] Y.Q. Qiao, J.P. Tu, Y.J. Mai, L.J. Cheng, X.L. Wang, C.D. Gu, *J. Alloys Compd.* 509 (2011) 7181.
- [53] J.Y. Xiang, J.P. Tu, Y.Q. Qiao, X.L. Wang, J. Zhong, D. Zhang, C.D. Gu, *J. Phys. Chem. C* 115 (2011) 2505.
- [54] Y. Lu, J.P. Tu, C.D. Gu, X.L. Wang, S.X. Mao, *J. Mater. Chem.* 21 (2011) 17988.
- [55] A.Q. Pan, J.-G. Zhang, G.Z. Cao, S.Q. Liang, C.M. Wang, Z.M. Nie, B.W. Arey, W. Xu, D.W. Liu, J. Xiao, G.S. Li, J. Liu, *J. Mater. Chem.* 21 (2011) 10077.
- [56] N.H. Idris, M.M. Rahman, J.-Z. Wang, Z.-X. Chen, H.-K. Liu, *Compos. Sci. Technol.* 71 (2011) 343.
- [57] X.Z. Ren, S.M. Hu, C. Shi, P.X. Zhang, Q.H. Yuan, J.H. Liu, *J. Solid State Electrochem.* 16 (2012) 2135.